Mutation rate of SARS-CoV-2 and emergence of mutators during experimental evolution

Massimo Amicone[1*], Vítor Borges[2*], Maria João Alves[3*], Joana Isidro[2*], Líbia Zé-Zé[3,4], Sílvia Duarte[5], Luís Vieira[5,6], Raquel Guiomar[7], João Paulo Gomes[2✉], Isabel Gordo[1✉]

*These authors contributed equally to this work.

[1]Instituto Gulbenkian de Ciência, Oeiras, Portugal.

[2]Bioinformatics Unit, Department of Infectious Diseases, National Institute of Health Doutor Ricardo Jorge (INSA), Lisbon, Portugal.

[3]Centre for Vectors and Infectious Diseases Research, Department of Infectious Diseases, National Institute of Health Doutor Ricardo Jorge (INSA), Águas de Moura, Portugal.

[4]BioISI - Biosystems & Integrative Sciences Institute, Faculty of Sciences, University of Lisbon, Portugal.

[5]Innovation and Technology Unit, Department of Human Genetics, National Institute of Health Doutor Ricardo Jorge (INSA), Lisbon, Portugal.

[6]Centre for Toxicogenomics and Human Health (ToxOmics), Genetics, Oncology and Human Toxicology, Nova Medical School|Faculdade de Ciências Médicas, Universidade Nova de Lisboa, Lisbon, Portugal.

[7]National Reference Laboratory for Influenza and other Respiratory Viruses, Department of Infectious Diseases, National Institute of Health Doutor Ricardo Jorge (INSA), Lisbon, Portugal.

✉e-mail: igordo@igc.gulbenkian.pt; j.paulo.gomes@insa.min-saude.pt

Abstract: 219 words; Main text: 4618 words; Figures: 5.

Abstract

Background and objectives. To understand how organisms evolve, it is fundamental to study how mutations emerge and establish. Here, we estimated the rate of mutation accumulation of SARS-CoV-2 *in vitro* and investigated the repeatability of its evolution when facing a new cell type but no immune or drug pressures.

Methodology. We performed experimental evolution with two strains of SARS-CoV-2, one carrying the originally described spike protein (CoV-2-D) and another carrying the D614G mutation that has spread worldwide (CoV-2-G). After 15 passages in Vero cells and whole genome sequencing, we characterized the spectrum and rate of the emerging mutations and looked for evidences of selection across the genomes of both strains.

Results. From the mutations accumulated, and excluding the genes with signals of selection, we estimate a spontaneous mutation rate of 1.25×10^{-6} nt^{-1} per infection cycle for both lineages of SARS-CoV-2. We further show that mutation accumulation is heterogeneous along the genome, with the spike gene accumulating mutations at rate five-fold higher than the genomic average. We also observe the emergence of mutators in the CoV-2-G background, likely linked to mutations in the RNA-dependent RNA polymerase and/or in the error-correcting exonuclease protein.

Conclusions and implications. These results provide valuable information on how spontaneous mutations emerge in SARS-CoV-2 and on how selection can shape its genome towards adaptation to new environments.

Lay summary

Mutation is the ultimate source of variation. We estimated how the SARS-COV-2 virus—cause of the COVID-19 pandemic—mutates. Upon infecting cells, its genome can change at a rate of 0.04 per replication. We also find that this rate can change and that its spike protein can adapt, even within few replications.

Background and objectives

Mutation is the principal process driving the origin of genetic diversity. The mutation rate is a function of replication fidelity and represents the intrinsic rate at which genetic changes emerge prior to selection. The substitution rate, instead, is a measure of

mutation accumulation in a given period of time and embeds the effects of selection[1]. These rates and the spectrum of the emerging mutations are fundamental parameters to understand how an organism evolves and how new variants are purged from, or establish in natural populations.

In DNA based microbes the genomic mutation rate per cell per generation, measured in laboratory conditions, is close to a constant[2]. On the other hand, for RNA viruses there is a remarkable variation in their replication fidelity[3,4]. The basic mutation rates, expressed as nucleotide substitutions per site per cell infection (s/n/c), vary between 10^{-6} to 10^{-3} for the several positive ssRNA viruses which have been studied[5]. Importantly, our current knowledge of the mutation rate of the human beta-coronavirus SARS-CoV-2, which is the cause of the COVID-19 pandemic[6], is based on estimates from different coronaviruses[5,7,8] and still lacks a direct quantification[9].

Laboratory evolution experiments with microbial populations allow to determine how fast mutations accumulate[10,11], and combining them with high-throughput sequencing is one of the best methods to estimate mutation rates, determine how they vary along the genome[12] and study the extent to which convergent evolution occurs[13,14].

Here, via experimental evolution of two natural variants of SARS-CoV-2[15] and whole genome sequencing, we characterized the spectrum and rates of their emerging mutations, and identified specific targets of selection. Such information is important for better understanding the basic biology of this virus and to quantify how predicable the evolution of strains with different transmission capabilities can be. It may also help determining some potential genomic constraints of the virus, which are key to the design of evolution proof vaccines and antiviral drugs.

Methodology

Virus growth and *in vitro* assay

Vero E6 (African green monkey, *Cercopithecus aethiops* kidney epithelial cells, ATCC® CRL 1586™) cells were cultured at 37ºC and 5% CO_2 in Minimum Essential Medium (MEM 1X, Gibco®) supplemented with 10% fetal bovine serum (FBS), penicillin (100 units/ml) and streptomycin (100 µg/ml) + fungizone. The two clinical isolates Portugal/PT0054/2020 and Portugal/PT1136/2020, isolated at the National Institute of

88 Health Doutor Ricardo Jorge (INSA), were used to produce the ancestors of the
89 experimental evolution, CoV-2-D and CoV-2-G, which seeded the two laboratory
90 evolution experiments. For this, the initial SARS-CoV-2 stock was produced by infecting
91 Vero E6 cells (freshly grown for 24 h) and incubating the cells for 72 h. The culture
92 supernatant was stored in aliquots at -80ºC. The $TCID_{50}$ of viral stock was calculated
93 according to the method of Reed and Muench[16]. All work with infectious SARS-CoV-2
94 strains was done inside a class III microbiological safety cabinet in a containment level 3
95 facility at the Centre for Vectors and Infectious Diseases Research (INSA).
96 From the stored stocks, two 96-well plates fully inoculated with 50 µl of Vero E6 cells
97 ($2.0x10^4$ cells) grown for 24 h were infected with 50 µl of the SARS-CoV-2 strains viral
98 suspension ($2.0x10^3$ viruses) at a multiplicity of infection (MOI) of 0.1. MEM
99 supplemented with 10% FBS, penicillin (100 units/ml) and streptomycin (100 µg/ml) +
100 fungizone was added to each well (50 µl) and the plates were incubated for 24 h. Each
101 well had a final volume of 150 µl. Every day, for 15 days, serial passages were done by
102 passaging 50 µl of the culture supernatant to 96-well plates (one for each SARS-CoV-2
103 strain under study) fully inoculated with 50 µl of Vero E6 cells ($2.0x10^4$ cells) using the
104 same procedure and incubated in the same conditions. At day 15, total nucleic acids
105 were extracted from 100 µl of viral suspension of each well in each plate (96 samples of
106 day 15th for each strain) using the automated platform NUCLISENS easyMAG
107 (Biomérieux). Confirmation of nucleic acid integrity and rough concentration estimative
108 was made before sequencing experiment by RT-qPCR of 8 random chosen samples from
109 each plate at day 15 (CoV-2-D and CoV-2-G) using Novel Coronavirus (2019-nCoV) RT-
110 PCR Detection Kit (Fosun Diagnostics). Samples from inoculation suspension (day 1)
111 were also analyzed. All samples presented values of 7-10 Ct (Cycle threshold). When we
112 infect the cells with $2x10^3$ particle forming units (PFU), after 24 h the number of PFUs is
113 around $2x10^6$. So, assuming no major fluctuations in the viral load of the transferred
114 suspension throughout the 15 passages and assuming a yield of approximately 1000
115 PFU/cell[9], the estimated number of replication cycles per passage is around 1
116 (i.e. $\ln(2x10^6/2x10^3)/\ln(10^3)$).
117
118 **SARS-CoV-2 genome sequencing and bioinformatics analysis**
119 Genome sequencing was performed at INSA following an amplicon-based whole-genome
120 amplification strategy using tiled, multiplexed primers[17], according to the ARTIC

121 network protocol (https://artic.network/ncov-2019;
122 https://www.protocols.io/view/ncov-2019-sequencing-protocol-bbmuik6w) with
123 slight modifications, as previously described[15]. Briefly, after cDNA synthesis, whole-
124 genome amplification was performed using two separate pools of tiling primers [pools 1
125 and 2; primers version V3 (218 primers) was used for all samples:
126 https://github.com/artic-network/artic-
127 ncov2019/tree/master/primer_schemes/nCoV-2019]. The two pools of multiplexed
128 amplicons were then pooled for each sample, followed by post PCR clean-up and Nextera
129 XT dual-indexed library preparation, according to the manufacturers' instructions.
130 Sequencing libraries were paired-end sequenced (2x150 bp) on an Illumina NextSeq 550
131 apparatus, as previously described[18]. Sequence read quality analysis and mapping was
132 conducted using the bioinformatics pipeline implemented in INSaFLU
133 (https://insaflu.insa.pt/; https://github.com/INSaFLU;
134 https://insaflu.readthedocs.io/en/latest/; as of 10 March 2021), which is a web-based
135 (and also locally installable) platform for amplicon-based next-generation sequencing
136 data analysis[18]. We performed raw reads quality analysis using FastQC v0.11.9
137 (https://www.bioinformatics.babraham.ac.uk/projects/fastqc), followed by quality
138 improvement using Trimmomatic v.0.27
139 (http://www.usadellab.org/cms/index.php?page=trimmomatic; HEADCROP:30 CROP:90
140 SLIDINGWINDOW:5:20 LEADING:3 TRAILING:3 MINLEN:35 TOPHRED33), with reads being
141 conservatively cropped 30 bp at both ends for primer clipping. Reference-based mapping
142 was performed against the Wuhan-Hu-1/2019 reference genome sequence
143 (https://www.ncbi.nlm.nih.gov/nuccore/MN908947.3; NC_045512.2) using the Burrow-
144 Wheeler Aligner (BWA_MEM) v.0.7.12 (r1039) (http://bio-bwa.sourceforge.net/)[19]
145 integrated in multisoftware tool Snippy (https://github.com/tseemann/snippy)
146 available in INSaFLU. The obtained median depth of coverage throughout the genome for
147 CoV-2-D and CoV-2-G samples (except two samples excluded due to low coverage) was
148 4807 (IQR=3969-5242) and 5154 (IQR=4802-5439), respectively. Variant (SNP/indels)
149 calling was performed over BAM files using LoFreq v.2.1.5 (*call* mode, including *--call-*
150 *indels*)[20], with indel qualities being assessed using Dindel[21]. Mutation frequency
151 analysis was dynamic and contingent on the depth of coverage of each processed site, e.g.
152 minor mutations at "allele" frequencies of 10%, 2% and 1% (minimum cut-off used) were
153 validated for sites with depth of coverage of at least 100-fold, 500-fold and 1000-fold,

154 respectively. The median depth coverage per site for all validated mutations in CoV-2-D
155 and CoV-2-G samples was 4219 (IQR=2508-6649) and 6424 (IQR=3076-10104),
156 respectively. In order to assess if proximal SNPs and/or indels belong to the same
157 mutational event (and thus, avoid overestimating the mutation rate), we identified all
158 consecutive mutations separated by ≤12 bp. The mutations more likely to represent a
159 single mutation event, i.e., those with similar frequencies (differing by ≤ 2.5%), were
160 further visually inspected using IGV (http://software.broadinstitute.org/software/igv/)
161 to confirm/exclude their co-localization in the same reads. In total, this curation led to the
162 identification 37 SNPs/indels that were collapsed into 13 complex or multi-nucleotide
163 polymorphisms (MNP). The effect of mutations on genes and predicted protein sequences
164 was determined using Ensembl Variant Effect Predictor (VEP) version 103.1
165 (https://github.com/Ensembl/ensembl-vep; available as a self-contained Docker
166 image)[22]. To obtain a refined annotation including all ORF1ab sub-peptides, the GFF3
167 genome annotation file (relative to the reference Wuhan-Hu-1/2019 genome of SARS-
168 CoV-2, acc. no. NC_045512.2) available in the coronapp COVID-19 genome annotator
169 (http://giorgilab.unibo.it/coronannotator/)[23]was adapted to generate an annotation
170 GTF file for input for the *--gtf* parameter. The parameter *--distance* was set to 0.
171 **Supplementary Table 1** summarizes all mutations detected in this study and their
172 distribution across clinical, ancestral cultures and end-point cultured lines (15th
173 passage). SARS-CoV-2 consensus sequences obtained directly from clinical samples for
174 CoV-2-D (Portugal/PT0054/2020) and CoV-2-G (Portugal/PT1136/2020) viruses are
175 available in GISAID under the accession numbers EPI_ISL_421457 and EPI_ISL_511683,
176 respectively. Reads generated at the end of the experimental evolution study were
177 deposited in the European Nucleotide Archive (ENA)
178 (https://www.ebi.ac.uk/ena/data/view/PRJEB43731).
179

180 **Simulations of the neutral mutation accumulation**

181 To obtain a non-equilibrium neutral expectation of the site frequency spectrum of
182 mutations, we performed forward-simulations to model mutation accumulation using
183 the mutation rate inferred from the experiment. We model an organism with a bi-allelic
184 genome of size L=30000 (~SARS-CoV-2). An initially isogenic population undergoes 15
185 cycles of growth, mutation and bottleneck, according to the following life cycle:
186 1. A clonal population starts with an inoculum size of 2000.

2. Each genome replicates X times. We assume the burst size X to be Poisson distributed with mean 1000.
3. For each of the replicating genomes we introduce a Poisson number of mutations with mean 0.1 (corresponding to a rate of 3.3×10^{-6} nt^{-1} $cycle^{-1}$). We assume mutations to emerge with uniform probability in the parental genome and we allow for back-mutation.
4. After replication and mutation, we sample 1/1000 of the individual genomes.
5. Repeat steps 2-4, 15 times.

We validated the simulation code by confirming expected outcomes: mutations accumulate linearly over time and the posterior estimation of the mutation rate retrieves the original value (bottom plot in **Fig. S3b**).

After 15 cycles we collect the artificial genomes from 100 independent simulations, and compute their site frequency spectrum as in the experiment. In order to test whether cross-well contamination could justify the observed site frequency distribution, we modified the previous algorithm by introducing migration. At each cycle t, after each bottleneck event, a fraction of viral genomes (m=0.1) is replaced by migrants sampled from a pool of genomes that have undergone t cycles of growth. The algorithm was written in R (version 3.6.1) and the results analyzed in RStudio[24].

Mutation accumulation rates in all, synonymous and non-synonymous sites

To quantify the rate at which mutations accumulate during the experiment, we compute $M_a(r) = \frac{\sum f_r}{P * L_r}$, where f_r is the frequency of all mutations observed in region r, P=15 the number of passages and L_r the length of region r. For the genome-wise mutation accumulation $L_r = 29903$, the entire genome of SARS-CoV-2. We also computed the mutation accumulation rates at synonymous and non-synonymous sites. In these cases, the synonymous rate is given by $M_a(r, syn) = \frac{\sum f_r}{P * L_r * p_{r,syn}}$, where $p_{r,syn}$ is the proportion of mutations in region r, leading to synonymous changes. Equivalently the non-synonymous rate is $M_a(r, n_syn) = \frac{\sum f_r}{P * L_r * p_{r,n_syn}}$. In practice, assume the region of interest has sequence r: ATGTTT. For each base we count the proportion of mutations that would change (or not) the corresponding amino acid. In the example $p_{r,n_syn} = 3/3 + 3/3 + 3/3 + 3/3 + 3/3 + 2/3 = 17/18$, 17 mutations out of the possible 18 are non-

218 synonymous and only one is synonymous (ATGTTc). Therefore, in this example, the total
219 size is $L_r = 6$, $p_{r,n_syn} = 17/18$ and $p_{r,syn} = 1/18$. Following this method, we calculated
220 the genome-wise and gene-specific mutation accumulation rates in all, synonymous or
221 non-synonymous sites (**Fig. 1-4** and **Fig. S4-5**). The genomic sequences of each region
222 were retrieved from NCBI (entry: NC_045512).
223

224 **pN/pS calculation and confidence interval**

225 Within a given region *r,* we computed *pN(r)* as the summed frequencies of all the
226 observed non-synonymous mutations over the number of all possible non-synonymous
227 changes in that region: $pN(r) = \frac{\sum f_r}{N_{r,n_syn}}$, where $N_{r,syn} = 3L_r p_{r,n_{syn}}$. Equivalently, we
228 computed the synonymous counterpart: $pS(r) = \frac{\sum f_r}{N_{r,syn}}$. In the previous example, within
229 the region r: ATGTTT, $N_{r,n_syn} = 17$ while $N_{r,syn} = 1$. Finally, the pN/pS statistics is the
230 ratio of pN and pS and its expected value is 1 under neutrality. To test the deviation from
231 1, we report the pN/pS together with its confidence interval. Being the pN/pS a ratio of
232 proportions, we computed the 95% confidence intervals of risk ratios, specifically as
233 $\left(e^{\ln\left(\frac{pN}{pS}\right)+z\sqrt{\frac{1-pN}{N_{n_syn}*pN}+\frac{1-pS}{N_{syn}*pS}}}, e^{\ln\left(\frac{pN}{pS}\right)-z\sqrt{\frac{1-pN}{N_{n_syn}*pN}+\frac{1-pS}{N_{syn}*pS}}}\right)$, with critical $z = 1.96$.

234 ## Results

235 **Experimental evolution design and ancestor backgrounds.**

236 Two SARS-CoV-2 viral strains were isolated from two non-related patients for continuous
237 propagation in Vero cells (see Methodology, **Fig. 1a**). These were chosen according to
238 their polymorphism at amino acid position 614 of the spike protein: CoV-2-D carries a D
239 and CoV-2-G carries a derived mutation which changes the D into a G. This D614G
240 mutation in spike emerged early in the pandemic, increased the infectivity of the virus
241 and became prevalent worldwide[25]. Here, we want to test for differences in their
242 mutation rates, spectrum and/or in the selective forces as the strains are propagated in
243 cells.

244 In order to discriminate *de novo* mutations from standing genetic variation, we identified
245 the mutations (relative to the Wuhan-Hu-1/2019 reference genome sequence, Wu et al.,
246 2020) that were already present at the start of our evolution experiment (see the list and
247 their frequencies in **Fig. S1**).

248 If the mutation rate is similar to that of the mouse hepatitis virus (MHV) or that of the
249 SARS-CoV (about $3.5x10^{-6}$ and $2.5x10^{-6}$ nt^{-1} $cycle^{-1}$, respectively)[5,7] hundreds of
250 mutations should accumulate, many of which are expected to be neutral but some could
251 reflect adaptation to the experimental conditions.
252
253 **Mutation accumulation and spectrum after 15 passages of SARS-CoV-2 evolution.**
254 We considered *de novo* mutations those that reached a frequency of at least 1%,
255 supported by a minimum of 10 reads and that were not detected in either the ancestor or
256 the original clinical isolate from which the ancestor was derived (full list in
257 **Supplementary Table 1**). Propagation of the 96 CoV-2-D derived lines resulted in 1753
258 *de novo* mutations, while the 96 lines derived from CoV-2-G resulted in 6181 *de novo*
259 mutations (n=94 as in two lines the sequencing had poor coverage) (**Fig. 1b**). The much
260 higher number of mutations in the CoV-2-G background, compared to CoV-2-D, is
261 explained by 15 of these lines where many more mutations were observed (**Fig. 1b**).
262 These lines, hereafter referred to as mutators, are characterized by a larger proportion
263 of SNPs compared to the non-mutator lines where, instead, deletions account for more
264 than 20% of all *de novo* mutations (**Fig. 1c**).
265 The frequency of mutator clones was estimated to be between 1 and 2% after 15 infection
266 cycles, since these were the frequencies measured for the vast majority of mutations
267 observed in the mutator lines. The genetic cause of the mutator phenotype is difficult to
268 determine but it could likely be hidden within the mutations that occurred in the RNA-
269 dependent RNA polymerase (Nsp12) and/or in the error-correcting exonuclease protein
270 (Nsp14)[8]. Indeed, looking at the mutations that are specific to the lineages with
271 mutators, we found 8 non-synonymous mutations in Nsp12 (one leading to a stop at
272 amino-acid 670) and 9 non-synonymous mutations in Nsp14 (one leading to a stop at
273 amino acid 78) (**Supplementary Tables 2-3**). Any of these mutations could potentially
274 lead to the observed change in mutation rate, but none of these have been associated with
275 an increased mutational load of the circulating viruses[27].
276 Next, we obtained the per-base per-passage rate at which mutations accumulated (M_a),
277 from the frequencies of the observed mutations. As a 24 h passage in our experiment
278 corresponds to ~1 cell replication cycle (see *Methodology*), we hereafter report such rate
279 of mutation accumulation per unit of replication cycle (nt^{-1} $cycle^{-1}$). Interestingly, the non-
280 mutator lines of CoV-2-G show a significantly lower accumulation rate compared to the

281 CoV-2-D lines ($P<10^{-6}$, Two-sample Kolmogorov-Smirnov test) (**Fig. 1d**). However, this
282 difference between the two backgrounds is more likely due to differences in selection
283 rather than differences in mutation rates, as we will explain later on.
284 The SNPs accumulated over 15 passages show that both genomic backgrounds have a
285 strong propensity to accumulate C->T mutations (**Fig. 1e**), a well-known bias of SARS-
286 CoV-2[28]. In the mutator lines, the main mutation bias changed from C->T to G->T (**Fig.**
287 **1e**), also observed in SARS-CoV-2 samples collected during the recent COVID-19
288 pandemic[29,30].
289 It is important to notice that, both the accumulation of mutations and the biases we
290 observe in the data (**Fig. 1b-e**) might have been shaped by selection and deviate from a
291 neutral rate and spectrum of mutations. In fact, on one hand positive selection can
292 increase the frequencies of beneficial mutations and on the other hand purifying selection
293 can purge the deleterious alleles. Therefore, we next looked for evidences of selection in
294 the mutation accumulation data.
295
296 **Signs of selection: Site frequency spectrum and heterogeneity across genes.**
297 In serial propagation experiments with SARS-CoV-2, it is extremely difficult to pick a
298 single virus[31]. In our experiment the effective population size is considerably large (see
299 *Methodology*), and thus could be insufficient to remove the effects of either positive or
300 negative selection[10]. Indeed, several patterns in the data indicate that selection played
301 a significant role in the experimentally evolved SARS-CoV-2 lines.
302 The distribution of allele frequencies in a sample, *i.e.* the site frequency spectrum, has a
303 well-known theoretical expectation under a simple equilibrium neutral model of
304 molecular evolution (Chap. 5 pg. 233 of B. Charlesworth & D. Charlesworth., 2010). But,
305 this distribution is sensitive to the action of selection and also to complex demographic
306 events, such as population bottlenecks. Given the bottlenecks occurring in our
307 experiments and the slow evolutionary time elapsed during the 15 infection cycles, the
308 neutral theoretical expectation at equilibrium may not apply. To obtain a non-
309 equilibrium expectation of the site frequency spectrum, we performed forward-
310 simulations (see *Methodology*). We assumed that neutral mutations occur at a rate of
311 3.3×10^{-6} nt^{-1} $cycle^{-1}$, similar to that estimated from the data, and simulated populations
312 evolving under neutrality. The site frequency spectrum of the mutations accumulated in
313 both CoV-2-D or CoV-2-G lines deviates significantly from the neutral expectation

314 predicted by the simulations (**Fig. 2a**). High frequency mutations are not expected under
315 neutrality (mutations with frequencies above 30% are reported in **Fig. S2**). To test
316 whether possible contamination among wells could explain the observed site frequency
317 spectrum, we performed additional simulations with migration (see *Methodology*). Even
318 when considering a migration rate of 10%, the neutral site frequency spectrum is still
319 incompatible with the experimental data (**Fig. S3a**). Furthermore, the 10% migration
320 between wells should not significantly change the estimation of mutation rate (**Fig. S3b**).
321 Thus, the data strongly suggest that positive selection has increased the frequency of
322 beneficial mutations and skewed the spectrum of the mutations (**Fig. 2a**).
323 A second evidence of selection comes from the considerable variation in the rate of
324 mutation accumulation observed across the SARS-CoV-2 genome (**Fig. 2b, Fig. S4**). When
325 excluding the mutator lines, the S gene, which codes for the spike protein, has the highest
326 rate of mutation accumulation among the different genes (**Fig. 2b**). Remarkably, the
327 spike accumulated $13.5\pm0.4\times10^{-6}$ $nt^{-1}/cycle^{-1}$ mutations in the CoV-2-G genotype
328 (excluding mutators), and $17.1\pm1.0\times10^{-6}$ in the CoV-2-D genotype, about five-fold the
329 corresponding genomic averages, suggesting the strong action of positive selection. In the
330 mutator lines, the spike gene evolved ~2 times faster than the non-mutators (**Fig. S4**).
331 This observation is in contrast with the expectation of a constant increase in mutation
332 rate across the genome and suggests that more complex selective forces might be acting
333 on the mutator phenotype (see the heterogeneity of the mutation rate across the CoV-2-
334 G mutator genome in **Fig. S4**). Overall, the data confirmed that selection has shaped the
335 way mutations accumulated. Therefore, in order to obtain a more accurate quantification
336 of the spontaneous rate of mutation, we performed a more systematic analysis of the sites
337 under selection.
338
339 **Identifying regions under selection**
340 From the frequencies of all mutations observed in the CoV-2-D and CoV-2-G non-mutator
341 lines, we computed an accumulation rate of 3.7×10^{-6} and 2.9×10^{-6} nt^{-1} $cycle^{-1}$, respectively
342 (**Fig. 1d**). Given that during our experiment, selection affected the allele frequencies (**Fig.**
343 **2**), such rates may deviate from the spontaneous mutation rates of the virus. In order to
344 attempt to estimate the spontaneous mutation rate we first focused on synonymous
345 mutations, which, if neutral, should accumulate at the rate at which they occur[33].
346 Focusing on the synonymous changes, we estimated a basic mutation rate of 3.8×10^{-6} nt^{-}

347 ^{1} cycle^{-1} for the CoV-2-D background and 1.2x10^{-6} nt^{-1} cycle^{-1} for the CoV-2-G (**Fig. S5a**).
348 However, the rate of non-synonymous mutation in CoV-2-D is lower than the
349 synonymous one (**Fig. S5a-b**), suggesting the action of purifying selection on non-
350 synonymous sites or positive selection on the synonymous sites, leading to their increase
351 in frequency[34,35]. To distinguish between the two cases, we compared the
352 accumulation rate of synonymous mutations in the entire genome (M_a^{Syn}), with the
353 accumulation rate of synonymous mutations excluding one gene at the time ($M_a^{Syn,\Delta g}$).
354 This approach revealed that a remarkable accumulation of synonymous mutations in the
355 Nsp6 gene led to the overestimation of the mutation rate in the CoV-2-D background (**Fig.
356 S5c**). In contrast, for the CoV-2-G background this approach indicates that the estimation
357 of M_a^{Syn}=1.2x10^{-6} nt^{-1} cycle^{-1} is homogeneous across the genome and can provide a first
358 estimation of its mutation rate (**Fig. S5d**).
359 Since the synonymous mutations alone could not provide a correct estimation of
360 mutation rate, we followed a different approach: identify the regions under selection in
361 either the CoV-2-D or CoV-2-G lines and exclude them from the estimation of the
362 spontaneous mutation rate. First, we compared the relative accumulation of non-
363 synonymous and synonymous mutations, via the *pN/pS* statistics (equivalent of *dN/dS*
364 for polymorphic samples, see *Methodology*). In the CoV-2-D background, the *pN/pS* of the
365 S and the Nsp6 genes significantly differ from 1 (**Fig. 3a**). The spike accumulated more
366 non-synonymous mutations consistent with the action of positive selection (*pN/pS*=4.4,
367 95% confidence interval: [1.4,13.9]), while the Nsp6 accumulated more synonymous
368 mutations, consistent with our previous findings (*pN/pS=0.02, 95%* confidence interval:
369 [0.00,0.12], **Fig. S5c**). In particular, the synonymous change A11041G was found in 88
370 evolved populations (out of 96), but also at frequency below our 1% threshold in the
371 ancestral population, suggesting that such mutation was incorrectly considered as *de
372 novo* and that the estimated mutation accumulation in Nsp6 was the resulting artifact.
373 Due to the limited number of mutations within each gene and the fact that we are
374 comparing evolving populations (rather than divergent species), the *pN/pS* may lack the
375 power to identify additional regions under selection[36]. To overcome this issue and to
376 identify additional genes affecting the estimation of the mutation rate, we computed the
377 rate of mutation accumulation excluding one gene at the time and compared this with the
378 entire genome (see *Methodology* and **Fig. 3c-d**). With this outlier-detecting method we
379 confirmed that the S and the Nsp6 genes affected the estimation of mutation rate in the

380 CoV-2-D strain, we could observe that the S gene is likely under selection also in the CoV-
381 2-G strain, and we identified Nsp3 as an additional region with a different rate of
382 mutation accumulation (**Fig. 3c-d**). In particular, Nsp3 accumulated fewer mutations
383 than the genomic average in both CoV-2-D and CoV-2-G strains, suggesting the action of
384 purifying selection (**Fig. 3c-d**).
385 Overall, we conclude that during our experiment, the spike protein was under strong
386 selection in both backgrounds, but also other genes biased the estimation of mutation
387 rate.
388
389 **Estimation of mutation rates and bias excluding genes with signs of selection**
390 Non-neutral processes have shaped the allele dynamics in our experiment. To get a more
391 realistic estimate of the mutation rate prior to selection, we excluded from the analysis
392 the Nsp3, Nsp6 and S genes, which have shown signs of selection in at least one of the two
393 backgrounds (**Fig. 3**). By doing this, we estimate a spontaneous mutation rate of
394 $1.3 \pm 0.2 \times 10^{-6}$ nt^{-1} $cycle^{-1}$ for the CoV-2-D background and $1.2 \pm 0.2 \times 10^{-6}$ nt^{-1} $cycle^{-1}$ for the
395 CoV-2-G (excluding mutators) (**Fig. 4a)**. The estimated mutation rate is similar across
396 backgrounds, suggesting that the previously observed differences were due to selection
397 (**Fig. 1d** and **S5**). Importantly, the estimated mutation rate of CoV-2-G is consistent with
398 that obtained using the synonymous mutations only (see **Fig. S5a**) and the estimated
399 mutation rate of CoV-2-D is consistent with that obtained using the synonymous
400 mutations only and excluding the Nsp6 (see **Fig. S5c**). We quantified again the relative
401 proportion of single nucleotide changes and confirmed that both backgrounds have a
402 spontaneous bias towards C>T mutations and the mutator changes this bias towards G>T
403 mutations (**Fig. 4b**).
404 Excluding the genes with signs of selection was our best attempt at quantifying the
405 spontaneous mutation rate of SARS-CoV-2. However, it is important to note that this may
406 still underestimate the real one due to the fact that we ignored mutations with a
407 frequency below the 1% threshold.
408
409 **Convergent targets of selection on Spike**
410 The spike protein showed clear signs of adaptation during our evolution experiment, so
411 we next focused on the specific sites under selection and compared them with the new
412 spike variants that spread in the human population. We first quantified the level of

413 convergence at the nucleotide and amino levels between CoV-2-D and CoV-2-G. We note
414 that convergence between the two backgrounds reflects true independent origin of the
415 mutations, as they were propagated and processed for sequencing independently. In
416 contrast, convergence within replicates of the same background could also result from
417 some possible cross-contamination or from undetected standing variation. At the amino
418 level, 20 specific sites and 3 regions were hit independently in both backgrounds (**Fig.
419 5a, Supplementary Table 4).** We find high evolutionary convergence at the S1/S2
420 cleavage site: three distinct deletions (675-QTQTN-679 del; 679-NSPRRAR-685 del and
421 679-NSPRRARSVA-688) emerge multiple times in both backgrounds. Such changes have
422 been previously shown to emerge rapidly in Vero cells and to be important for the virus
423 cell tropism[37]. Apart from these deletions, mutations of the Arginine 682 were also
424 highly convergent, most likely because they trigger a similar functional effect, i.e., knock
425 out of the furin cleavage site[38]. Notably, another deletion in this region (678-
426 TNSPRRARS-686 del) was frequently observed, still it was exclusive of CoV-2-D lines (*n*=
427 58), suggesting that the conformation changes mediated by D614G may influence the
428 directionality of the evolution towards the knock out of the furin-cleavage site[39].
429 Some level of evolutionary convergence could also be found for the structural genes N, E
430 and M suggesting that adaptation could also have occurred in these genes
431 (**Supplementary Table 5**).
432 The inferred mutators in the CoV-2-G background also carry many mutations in the spike
433 protein including in the receptor binding domain -RBD- (amino acid changes at positions
434 328, 339, 364, 416, 454, 465, 474, 479, 482, 522 and 524) and multi cleavage site regions
435 (positions 798 and 799) (**Fig. 5b**).
436 When scrutinizing the list of non-synonymous mutations in the spike that emerged
437 during our experiment in both backgrounds or in the mutator lines, we found 24 amino-
438 acid changes that were also observed in the natural population of SARS-CoV-2 (until the
439 24th of October 2021; https://nextstrain.org/ncov/gisaid/global) (full list reported in
440 **Supplementary Table 6** and highlighted in bold in **Fig. 5**). Among these, we observed
441 the mutations H655Y (present in the variant of concern Gamma, lineage P.1, originated
442 in Brazil), D215G (present in the variant of concern Beta, lineage B.1.351, firstly identified
443 in South Africa) and D253G (found in lineage B.1.426, mostly detected in the US) (**Fig.
444 5b**)[40].

Conclusions and implications

The SARS-CoV-2 beta-coronavirus, first observed in the Wuhan province of China[6], has infected at least 246 million people causing more than a 5 million toll of deaths in the human population (as of 2 November 2021; https://covid19.who.int/). Since it was first sequenced[26] the virus has been accumulating 0.44 substitutions per week at close to linear rate. Here we estimate its rate of spontaneous mutation to be of the order of 10^{-6} per base per cell infection, consistent with previous estimations in other coronaviruses[9]. New beneficial mutations did spread to high frequencies and considerable convergent evolution was detected across different genomic backgrounds. We also observe viral populations with an increased mutation rate emerging just within 15 days of propagation in cells. This suggests that the mutation rate of SARS-CoV-2 can increase without significant loss of viability (at least in the short run) and that strategies to reduce viral fitness using mutagens should be tested with precaution[41,42].

Overall the results show the remarkable ability of SARS-CoV-2 to adapt to new environments, in particular via convergent evolution of its spike protein in cells, and is fully consistent to its rapid adaptation to different hosts[43,44].

Data and materials availability

SARS-CoV-2 consensus genome sequences obtained directly from clinical samples for CoV-2-D (Portugal/PT0054/2020) and CoV-2-G (Portugal/PT1136/2020) viruses are available in GISAID under the accession numbers EPI_ISL_421457 and EPI_ISL_511683, respectively. Reads generated throughout the experimental evolution in this study were deposited in the European Nucleotide Archive (ENA) (https://www.ebi.ac.uk/ena/data/view/PRJEB43731). The code for the neutral model was deposited on https://github.com/AmiconeM/neutralviralpassage.

Acknowledgments: We would like to thank the personnel of the IGC Genomic Facility for their assistance.

Funding: M.A. was supported by "Fundação para a Ciência e Tecnologia" (FCT), fellowships PD/BD/138735/2018, respectively. Research was supported by FCT Project PTDC/BIA-EVL/31528/2017 to I.G. and by funds from Portuguese NIH.

Author contributions: IG, MJA and JPG designed the project. MJA and LZZ performed the culture and RNA extraction experiments. VB and JI performed the pre-sequencing wet-lab procedures, bioinformatic analysis and data analysis. SD and LV performed and supervised the wet-lab sequencing procedures. IG, MA performed the data analysis and the simulations. MJA, LV and JPG provided materials and reagents. IG wrote the initial draft of manuscript. VB, MJA, MA and JI contributed equally to this work. All authors contributed in the final writing of the manuscript and gave final approval for publication.

Ethical statement: The Portuguese NIH is authorized by the Portuguese Authorities' (General-Directorate of Health and the Authority for Working Conditions) to handle and propagate Risk group 2 and 3 microorganisms. All culture procedures were performed inside a class III microbiological safety cabinet in a containment level 3 facility. This study is covered by the ethical approval issued by the Ethical Committee ("Comissão de Ética para a Saúde") of the Portuguese National Institute of Health.

Competing interests: The authors declare no competing interests.

Additional information: Supplementary information is available for this paper. Correspondence and requests for materials should be addressed to igordo@igc.gulbenkian.pt; j.paulo.gomes@insa.min-saude.pt.

499 ## References

500 1. Lin JJ, Bhattacharjee MJ, Yu CP *et al.* Many human RNA viruses show extraordinarily
501 stringent selective constraints on protein evolution. *Proc Natl Acad Sci U S A* 2019, DOI:
502 10.1073/pnas.1907626116.

503 2. Drake JW. A constant rate of spontaneous mutation in DNA-based microbes. *Proc Natl*
504 *Acad Sci U S A* 1991, DOI: 10.1073/pnas.88.16.7160.

505 3. Drake JW. Rates of spontaneous mutation among RNA viruses. *Proc Natl Acad Sci U S*
506 *A* 1993, DOI: 10.1073/pnas.90.9.4171.

507 4. Drake JW, Charlesworth B, Charlesworth D *et al.* Rates of spontaneous mutation.
508 *Genetics* 1998, DOI: 10.1093/genetics/148.4.1667.

509 5. Sanjuán R, Nebot MR, Chirico N *et al.* Viral Mutation Rates. *J Virol* 2010, DOI:
510 10.1128/jvi.00694-10.

511 6. Zhu N, Zhang D, Wang W *et al.* A Novel Coronavirus from Patients with Pneumonia in
512 China, 2019. *N Engl J Med* 2020, DOI: 10.1056/nejmoa2001017.

513 7. Eckerle LD, Lu X, Sperry SM *et al.* High Fidelity of Murine Hepatitis Virus Replication
514 Is Decreased in nsp14 Exoribonuclease Mutants. *J Virol* 2007;**81**:12135–44.

515 8. Eckerle LD, Becker MM, Halpin RA *et al.* Infidelity of SARS-CoV Nsp14-exonuclease
516 mutant virus replication is revealed by complete genome sequencing. *PLoS Pathog*
517 2010;**6**:1–15.

518 9. Bar-On YM, Flamholz A, Phillips R *et al.* Sars-cov-2 (Covid-19) by the numbers. *Elife*
519 2020, DOI: 10.7554/eLife.57309.

520 10. Chao L. Fitness of RNA virus decreased by Muller's ratchet. *Nature* 1990, DOI:
521 10.1038/348454a0.

522 11. Duarte E, Clarke D, Moya A *et al.* Rapid fitness losses in mammalian RNA virus clones
523 due to Muller's ratchet. *Proc Natl Acad Sci U S A* 1992, DOI: 10.1073/pnas.89.13.6015.

524 12. Lynch M, Ackerman MS, Gout JF *et al.* Genetic drift, selection and the evolution of the
525 mutation rate. *Nat Rev Genet* 2016, DOI: 10.1038/nrg.2016.104.
526 13. Bull JJ, Badgett MR, Wichman HA *et al.* Exceptional convergent evolution in a virus.
527 *Genetics* 1997, DOI: 10.1093/genetics/147.4.1497.
528 14. Tenaillon O, Rodríguez-Verdugo A, Gaut RL *et al.* The molecular diversity of adaptive
529 convergence. *Science (80-)* 2012, DOI: 10.1126/science.1212986.
530 15. Borges V, Isidro J, Cortes-Martins H *et al.* Massive dissemination of a SARS-CoV-2
531 Spike Y839 variant in Portugal. *Emerg Microbes Infect* 2020, DOI:
532 10.1080/22221751.2020.1844552.
533 16. Reed LJ, Muench H. A simple method of estimating fifty per cent endpoints. *Am J*
534 *Epidemiol* 1938, DOI: 10.1093/oxfordjournals.aje.a118408.
535 17. Quick J, Grubaugh ND, Pullan ST *et al.* Multiplex PCR method for MinION and
536 Illumina sequencing of Zika and other virus genomes directly from clinical samples. *Nat*
537 *Protoc* 2017, DOI: 10.1038/nprot.2017.066.
538 18. Borges V, Pinheiro M, Pechirra P *et al.* INSaFLU: An automated open web-based
539 bioinformatics suite "from-reads" for influenza whole-genome-sequencing-based
540 surveillance. *Genome Med* 2018, DOI: 10.1186/s13073-018-0555-0.
541 19. Li H, Durbin R. Fast and accurate short read alignment with Burrows-Wheeler
542 transform. *Bioinformatics* 2009, DOI: 10.1093/bioinformatics/btp324.
543 20. Wilm A, Aw PPK, Bertrand D *et al.* LoFreq: A sequence-quality aware, ultra-sensitive
544 variant caller for uncovering cell-population heterogeneity from high-throughput
545 sequencing datasets. *Nucleic Acids Res* 2012, DOI: 10.1093/nar/gks918.
546 21. Albers CA, Lunter G, MacArthur DG *et al.* Dindel: Accurate indel calls from short-read
547 data. *Genome Res* 2011, DOI: 10.1101/gr.112326.110.
548 22. McLaren W, Gil L, Hunt SE *et al.* The Ensembl Variant Effect Predictor. *Genome Biol*

549 2016, DOI: 10.1186/s13059-016-0974-4.

550 23. Mercatelli D, Triboli L, Fornasari E *et al.* Coronapp: A web application to annotate
551 and monitor SARS-CoV-2 mutations. *J Med Virol* 2021;**93**:3238–45.

552 24. Core R Team. A Language and Environment for Statistical Computing. *R Found Stat*
553 *Comput* 2019.

554 25. Korber B, Fischer WM, Gnanakaran S *et al.* Tracking Changes in SARS-CoV-2 Spike:
555 Evidence that D614G Increases Infectivity of the COVID-19 Virus. *Cell* 2020, DOI:
556 10.1016/j.cell.2020.06.043.

557 26. Wu F, Zhao S, Yu B *et al.* A new coronavirus associated with human respiratory
558 disease in China. *Nature* 2020, DOI: 10.1038/s41586-020-2008-3.

559 27. Eskier D, Suner A, Oktay Y *et al.* Mutations of SARS-CoV-2 nsp14 exhibit strong
560 association with increased genome-wide mutation load. *PeerJ* 2020, DOI:
561 10.7717/peerj.10181.

562 28. Matyášek R, Kovařík A. Mutation patterns of human SARS-CoV-2 and bat RATG13
563 coronavirus genomes are strongly biased towards C>U transitions, indicating rapid
564 evolution in their hosts. *Genes (Basel)* 2020, DOI: 10.3390/genes11070761.

565 29. Yi K, Kim SY, Bleazard T *et al.* Mutational spectrum of SARS-CoV-2 during the global
566 pandemic. *Exp Mol Med* 2021;**53**:1229–37.

567 30. Tonkin-Hill G, Martincorena I, Amato R *et al.* Patterns of within-host genetic
568 diversity in SARS-COV-2. *Elife* 2021, DOI: 10.7554/eLife.66857.

569 31. Szemiel AM, Merits A, Orton RJ *et al.* In vitro selection of Remdesivir resistance
570 suggests evolutionary predictability of SARS-CoV-2. *PLOS Pathog* 2021, DOI:
571 10.1371/journal.ppat.1009929.

572 32. JIGGINS C. Elements of Evolutionary Genetics. B. Charlesworth & D. Charlesworth.
573 Roberts & Company. 2010. 768 pages. ISBN 9780981519425. Price $80 (hardback).

574 *Genet Res (Camb)* 2010, DOI: 10.1017/s001667231000042x.

575 33. Kimura M. Evolutionary rate at the molecular level. *Nature* 1968, DOI:

576 10.1038/217624a0.

577 34. Novella IS, Zárate S, Metzgar D *et al.* Positive selection of synonymous mutations in

578 vesicular stomatitis virus. *J Mol Biol* 2004, DOI: 10.1016/j.jmb.2004.08.003.

579 35. Zanini F, Neher RA. Quantifying Selection against Synonymous Mutations in HIV-1

580 env Evolution . *J Virol* 2013, DOI: 10.1128/jvi.01529-13.

581 36. Kryazhimskiy S, Plotkin JB. The population genetics of dN/dS. *PLoS Genet* 2008, DOI:

582 10.1371/journal.pgen.1000304.

583 37. Sasaki M, Uemura K, Sato A *et al.* SARS-CoV-2 variants with mutations at the S1/ S2

584 cleavage site are generated in vitro during propagation in TMPRSS2-deficient cells. *PLoS*

585 *Pathog* 2021;**17**:1–17.

586 38. Liu Z, Zheng H, Lin H *et al.* Identification of Common Deletions in the Spike Protein of

587 Severe Acute Respiratory Syndrome Coronavirus 2. *J Virol* 2020, DOI:

588 10.1128/jvi.00790-20.

589 39. Gobeil SMC, Janowska K, McDowell S *et al.* D614G Mutation Alters SARS-CoV-2 Spike

590 Conformation and Enhances Protease Cleavage at the S1/S2 Junction. *Cell Rep* 2021,

591 DOI: 10.1016/j.celrep.2020.108630.

592 40. Makoni M. South Africa responds to new SARS-CoV-2 variant. *Lancet (London,*

593 *England)* 2021, DOI: 10.1016/S0140-6736(21)00144-6.

594 41. Jensen JD, Stikeleather RA, Kowalik TF *et al.* Imposed mutational meltdown as an

595 antiviral strategy. *Evolution (N Y)* 2020, DOI: 10.1111/evo.14107.

596 42. Jensen JD, Lynch M. Considering mutational meltdown as a potential SARS-CoV-2

597 treatment strategy. *Heredity (Edinb)* 2020, DOI: 10.1038/s41437-020-0314-z.

598 43. Gu H, Chen Q, Yang G *et al.* Adaptation of SARS-CoV-2 in BALB/c mice for testing

599 vaccine efficacy. *Science (80-)* 2020, DOI: 10.1126/science.abc4730.

600 44. Tegally H, Wilkinson E, Giovanetti M *et al.* Emergence of a SARS-CoV-2 variant of

601 concern with mutations in spike glycoprotein. *Nature* 2021, DOI: 10.1038/s41586-021-

602 03402-9.

603

604 **Figures**

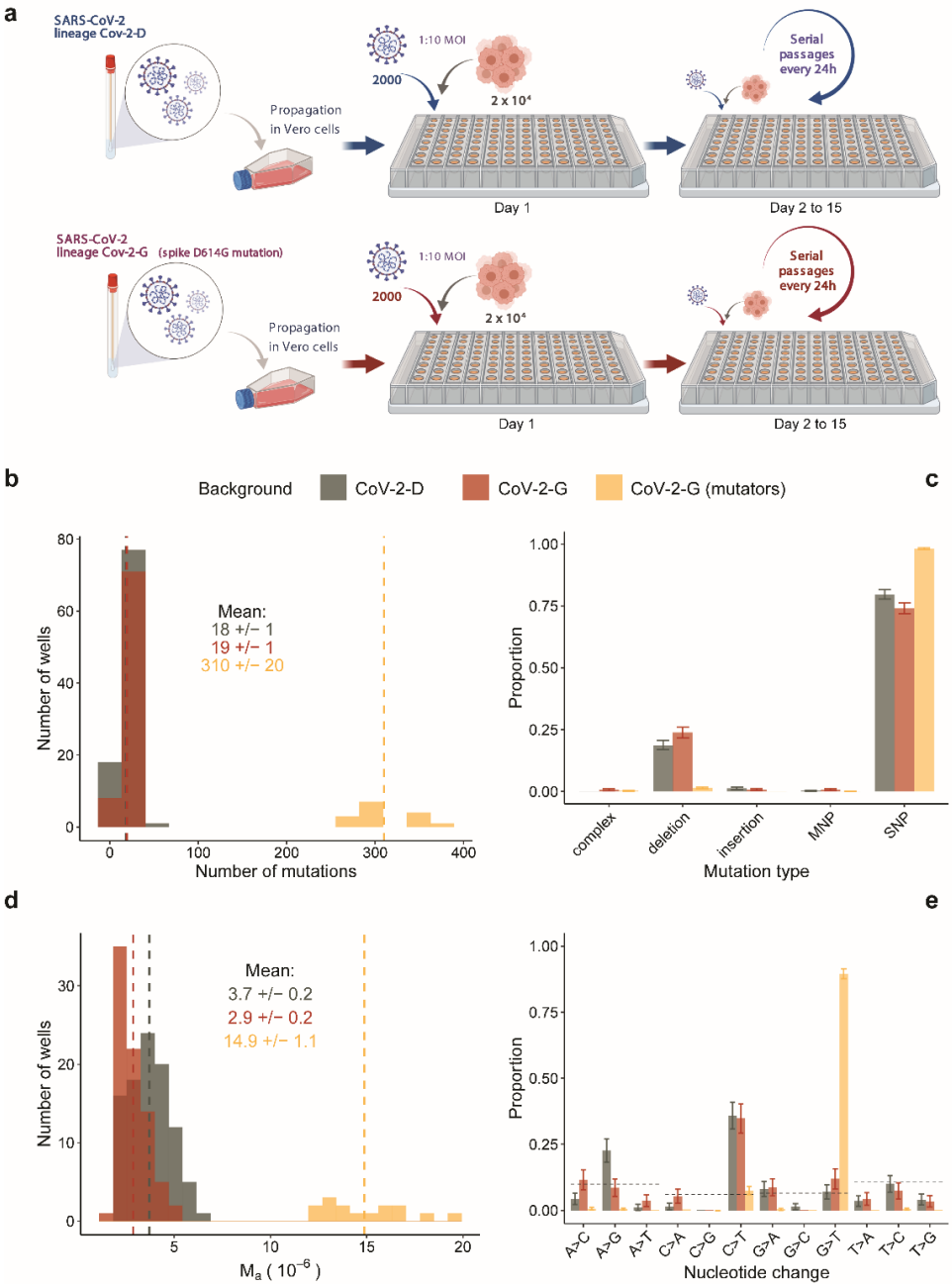

605

606 **Fig. 1| Experimental design and mutation accumulation after 15 passages of SARS-**
607 **CoV-2 evolution. a,** Schematic of the experimental design of the mutation accumulation
608 experiments where two viral backgrounds were propagated in Vero cells (figure created
609 with BioRender.com). **b,** Number of mutations observed in each well and group. 15 lines of
610 the CoV-2-G background accumulated a larger number of mutations and thus were defined
611 as mutators (gold). The means of each group are presented by vertical dashed lines and
612 reported in the figure (+/- 2SEM). **c,** Proportion of mutation types in each group. Complex
613 mutations and multi-nucleotide polymorphisms (MNP) are defined in the *Methodology*. **d,**
614 Mutation accumulation per base per infection cycle (M_a) was calculated by summing the
615 observed mutation frequencies as: $M_a = \frac{\sum f}{P*G}$, where P is the number of passages (P=15)
616 and G is the SARS-CoV-2 genome length (G=29903). The means of each group are
617 presented by vertical dashed lines and reported in the figure (+/- 2SEM). **e,** Proportion of
618 observed nucleotide changes. Dashed lines indicate the expectation given the genome
619 composition under equal mutation probability for each type of nucleotide change. Vertical
620 bars in panels **c** and **e** represent the 95% confidence interval computed as $p \pm$
621 $z\sqrt{\frac{p(1-p)}{N}}, z = 1.96$.
622

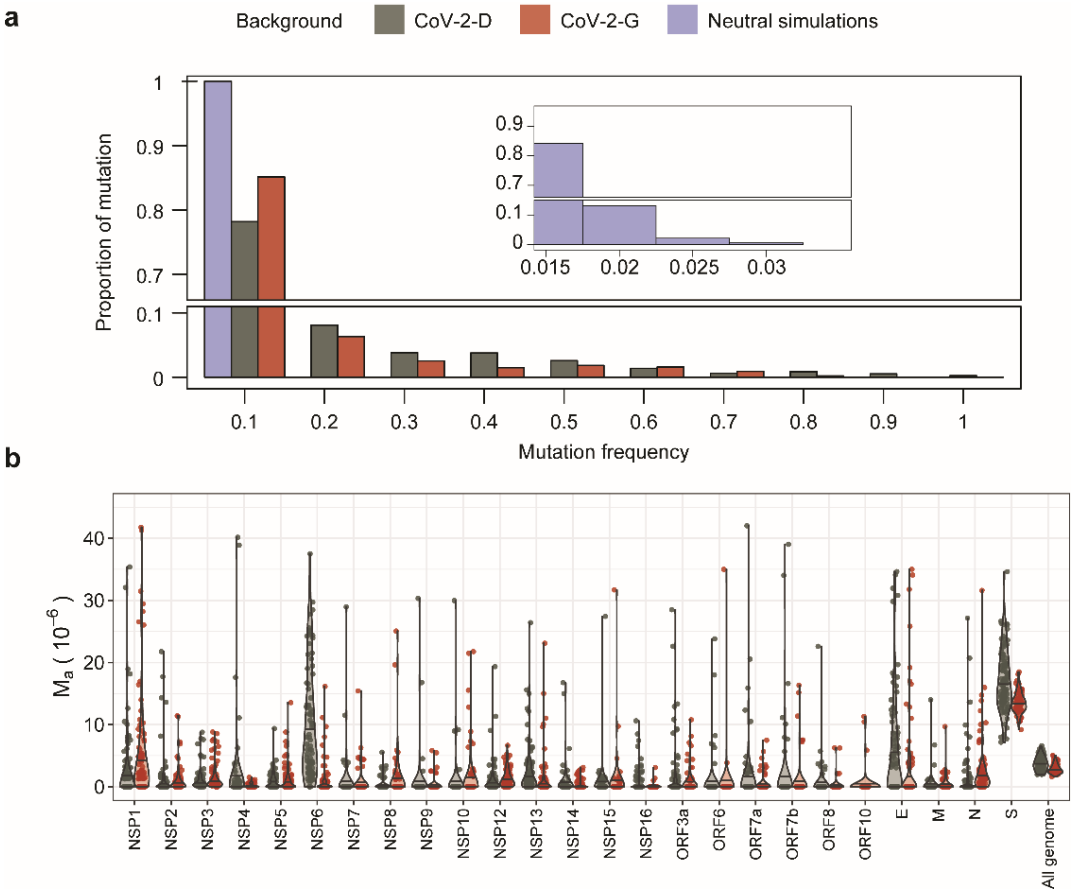

Fig. 2| Site frequency spectrum and heterogeneity across genes. a, Proportion of mutations with a given frequency after 15 cycles of propagation in the CoV-2-D and CoV-2-G genetic background or under a simulated neutral model of mutation accumulation. The bump observed at high frequencies in the data is not compatible with the expectation of the neutral model. **b,** Per-base mutation accumulation (M_a) computed for each gene and for the entire genome shows heterogeneity. The spike gene has the largest accumulation rate in both backgrounds ($M_a^{(S)} = 17.1 \pm 1.0, 13.5 \pm 0.4 \cdot 10^{-6}$, for the CoV-2-D and CoV-2-G respectively), which is more than 4 times their genomic average. For resolution purposes, few outliers with M_a above 45 are not shown (see full set in **Fig. S4**).

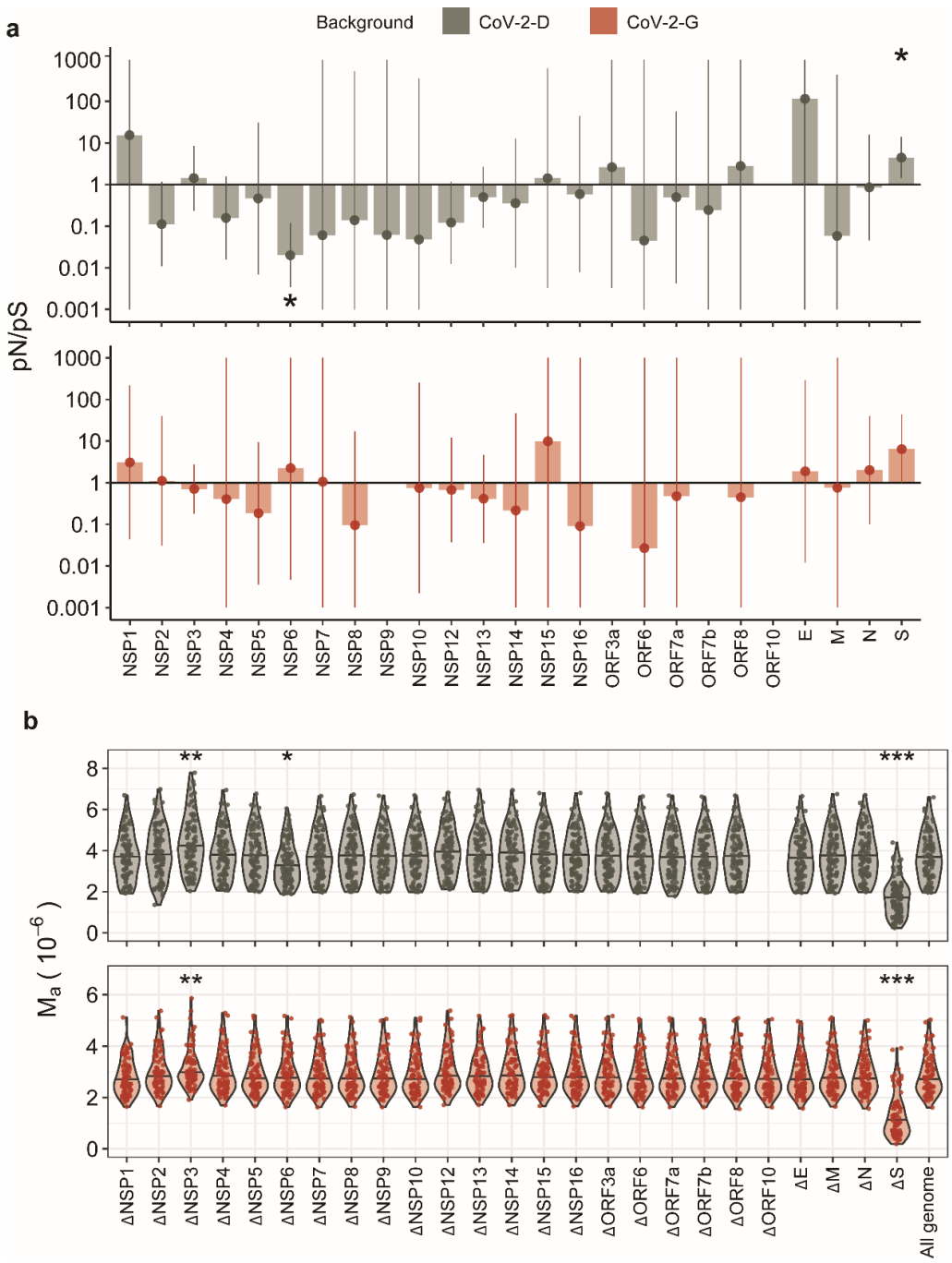

Fig. 3| Gene-wise signs of selection. a, The relative proportion of non-synonymous to synonymous polymorphism, *pN/pS,* was computed for each gene and genetic background (see *Methodology*). The horizontal line indicates the expectation under neutrality (pN/pS=*1*), values above suggest positive selection while values below suggest purifying selection. Vertical bars show the 95% confidence intervals and the stars indicate the genes where such interval does not include 1. For the sake of resolution, we show the confidence intervals within the $[10^{-3}, 10^{3}]$ range. **b,** Identifying the genes that affect the estimation of mutation rate. Per-base mutation accumulation

(M_a) was computed for the entire genome or by excluding each gene on at the time (e.g. ΔS). The stars indicate the cases where removing the gene leads to an estimation of M_a significantly different from the all genome (non-parametric Wilcox test, p-value < 0.05 (*), 0.01 (**) or 0.001 (***)).

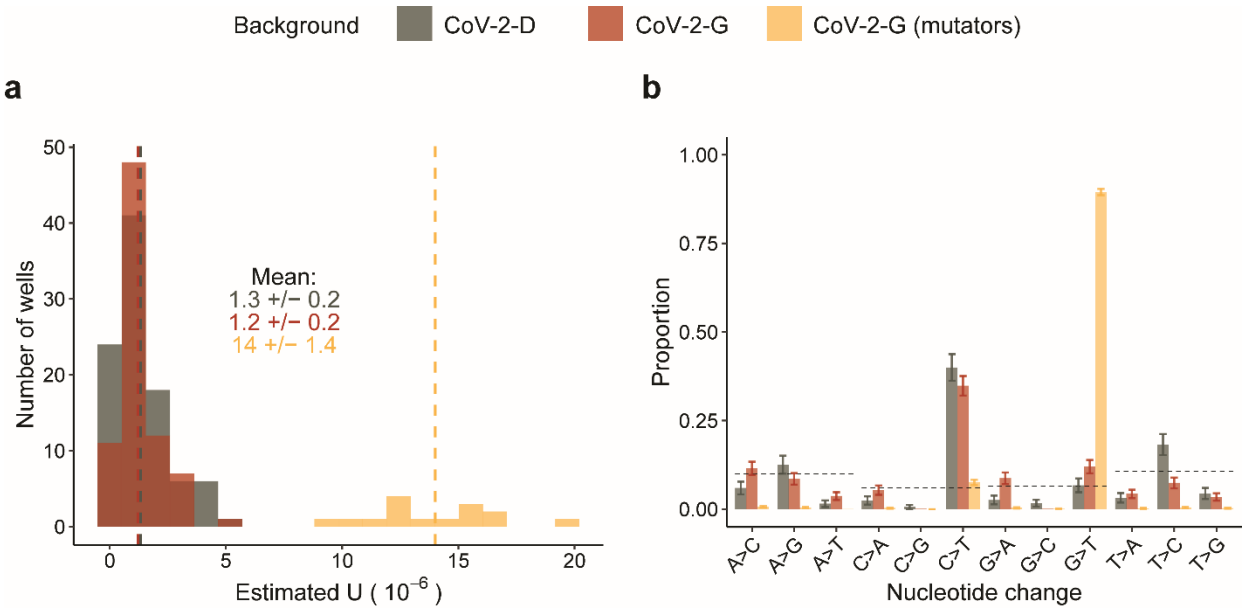

Fig. 4| Estimation of mutation rates and bias excluding outlier genes. a, The per-base per-infection cycle mutation rate was calculated by summing the observed mutation frequencies as: $U = \frac{\sum f}{P*G}$, where P is the number of passages (P=15) and G is the length of SARS-CoV-2 genome excluding the Nsp3, Nsp6 and Spike genes (29903-5835-870-3822=19376). The means of each group are presented as vertical dashed lines and reported in the figure (+/- 2SEM). **b,** Proportion of nucleotide changes observed excluding the Nsp3, Nsp6 and Spike genes. Dotted lines indicate the expectation given the genome composition under equal mutation probability for each type of nucleotide change. Vertical bars represent the 95% confidence interval computed as $p \pm z\sqrt{\frac{p(1-p)}{N}}, z = 1.96$.

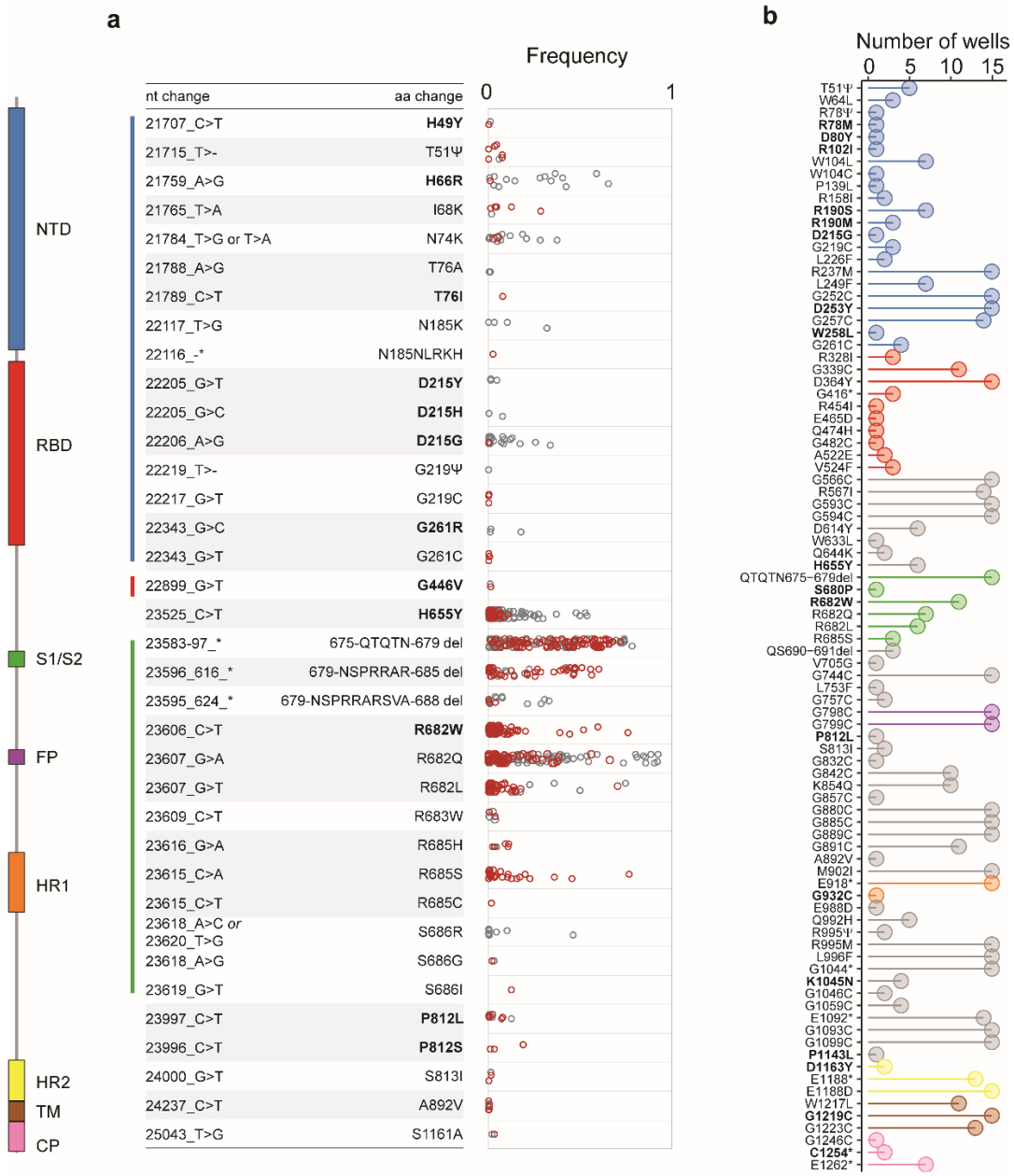

Fig. 5| Convergent evolution in the Spike gene. a, Mutations on S observed in both CoV-2-D and CoV-2-G backgrounds and their frequencies in each well (open circles). **b,** Non-synonymous mutations on the spike detected in the populations where the mutators were observed (number of wells on the X-axis). The color annotation represents the N-terminal domain (NTD, 14–305), the receptor-binding domain (RBD, 319–541), the cleavage site (S1/S2, 669-688), the fusion peptide (FP, 788–806), the heptapeptide repeat sequences (HR1, 912–984 and HR2, 1163–1213), the TM domain (1213–1237), and cytoplasm domain (CP, 1237–1273). Amino acids changes in bold were also observed in the human population (as of 24 October 2021; https://nextstrain.org/ncov/gisaid/global) (full list in **Supplementary Table 6**).